

Heavy-fermion behavior in YbPtIn

D. Kaczorowski*

*W. Trzebiatowski Institute of Low Temperature and Structure Research, Polish Academy of Sciences, P.O. Box 1410,
50-950 Wrocław, Poland*

B. Andraka and R. Pietri

Department of Physics, University of Florida, P.O. Box 118440, Gainesville, Florida 32611

T. Cichorek

*W. Trzebiatowski Institute of Low Temperature and Structure Research, Polish Academy of Sciences, P.O. Box 1410,
50-950 Wrocław, Poland*

V. I. Zaremba

Department of Inorganic Chemistry, Lviv State University, 290 005 Lviv, Ukraine

(Received 29 December 1999)

The ytterbium compound YbPtIn has been studied by means of single-crystal x-ray diffraction, magnetic susceptibility, magnetization, heat capacity, electrical resistivity, and magnetoresistivity measurements, performed down to 100 mK in fields up to 14 T. The magnetic properties of YbPtIn are governed by the presence of the magnetic moments of Yb^{3+} ions, which order magnetically at low temperatures. Strongly enhanced electronic specific heat, highly reduced magnetic entropy, and characteristic Kondo-like behavior of the resistivity and the magnetoresistivity allow classifying YbPtIn as a heavy-fermion system.

I. INTRODUCTION

In recent years one observes a rapidly growing interest in a study of ytterbium-based intermetallics, which are considered as hole counterparts to isostructural cerium compounds. Indeed, with its $4f^{14}$ configuration the Yb^{2+} ion is nonmagnetic, as the Ce^{4+} ion with the $4f^0$ configuration, and the Yb^{3+} ion with the $4f^{13}$ configuration carries a magnetic moment like the Ce^{3+} ion with the $4f^1$ configuration. Moreover, Yb can also exhibit intermediate valence states due to charge fluctuations between the two terminal configurations. It is commonly believed that the ground-state behavior in ytterbium compounds is governed mainly by the interaction of $4f$ electronic states with s, p, d states of neighboring ligands, as is the case for their cerium analogs. However, due to smaller spatial extent of Yb $4f$ orbitals with respect to Ce $4f$ orbitals, the f - spd hybridization in Yb-based compounds is usually weaker than in corresponding Ce-based phases and therefore most Yb intermetallics exhibit stable valence.

The most extensively studied family of ytterbium compounds is probably a series of equiatomic ternary phases with the general formula YbTM , where T stands for a d -electron transition metal and M is a p -electron metal or metalloid. Among these ternaries many phases are nonmagnetic, as, for example, stannides YbTSn and bismuthides YbTBi with T =noble metals.¹ A few compounds show intermediate valence properties, and the best prominent examples are YbCuAl (Ref. 2) and YbPdIn (Ref. 3). Dense Kondo systems are also well established, which usually order magnetically at low temperatures, e.g., ferromagnetic YbNiSn (Ref. 4) or antiferromagnetic YbPtGa (Ref. 5). Apparently, relatively few Yb phases exhibit heavy-fermion phenomena. Within the YbTM series these are YbNiAl ,⁶

YbPdSb ,⁷ YbPdBi ,^{1,7,8} and YbPtBi ,⁹ which also order antiferromagnetically with T_N of the order of 1 K. Spectacularly, YbPtBi exhibits a huge electronic specific heat coefficient γ of about 8 J/mol K².

In this paper we report on the crystal structure and magnetic, thermal, and electrical transport behavior of a new equiatomic ytterbium compound YbPtIn. A short account on a part of this work has recently been presented in a conference article.¹⁰ When writing this paper we become aware of a similar study of YbPtIn carried out by an independent research group.¹¹

II. EXPERIMENT

The starting materials for the preparation of YbPtIn and LaPtIn were ytterbium and lanthanum ingots (Johnson Matthey), platinum plate (Degussa), and indium teardrops (Johnson Matthey), all with stated purities greater than 99.9%. The elemental components were mixed in the ideal 1:1:1 atomic ratio and arc melted in a titanium-gettered argon atmosphere. The buttons were subsequently placed in a tantalum container, sealed in an evacuated silica tube, and annealed at 800 °C for 4 days. Thereafter the ampoule was cooled down to room temperature at a rate of 10 °C per hour. The purity of the so-obtained samples was checked by x-ray diffraction using an automatic powder diffractometer DRON-3M with $\text{CuK}\alpha$ radiation. The x-ray diffraction pattern was fully indexed in a hexagonal system with the lattice parameters $a=753.8(1)$ pm, $c=376.5(1)$ pm for YbPtIn and $a=768.8(1)$ pm, $c=412.9(1)$ pm for LaPtIn.

Several small single crystals of YbPtIn were isolated from the crushed button. They had an irregular plateletlike shape, a metallic luster, and were stable on air. The microprobe

TABLE I. Crystallographic data for YbPtIn [$a=753.5(2)$ pm, $c=376.3(1)$ pm, $V=0.1850(1)$ nm³, space group $P\bar{6}2m$, $Z=3$]. The form of the anisotropic displacement parameter is $\exp[-\frac{1}{4}(h^2a^{*2}B_{11} + k^2b^{*2}B_{22} + l^2c^{*2}B_{33} + 2hka^*b^*B_{12} + 2hla^*c^*B_{13} + 2klb^*c^*B_{23})]$, where a^* , b^* , and c^* are the reciprocal lattice parameters. $B_{13}=B_{23}=0$. B_{eq} stands for the isotropic thermal parameter defined as one-third of the trace of the orthogonalized B_{ij} tensor. No. of measured reflections=220, No. of unique reflections=138, No. of variables=14, absorption coefficient=1077.65 cm⁻¹, extinction coefficient=0.0028(4), $R_\sigma=0.0354$, $R_{eq}=0.0376$, $R_f=0.0517$, $R_w=0.0525$, goodness of fit=1.270.

Atom	Site	Positional parameters			Displacement parameters (10 ⁻² nm ²)				
		x	y	z	B_{11}	B_{22}	B_{33}	B_{12}	B_{eq}
Yb	3f	0.5959(4)	0	0	0.46(8)	0.52(10)	0.26(11)	$\frac{1}{2}B_{22}$	0.40(7)
In	3g	0.2637(6)	0	0.5	0.35(12)	0.26(15)	0.40(16)	$\frac{1}{2}B_{22}$	0.35(11)
Pt1	2d	1/3	2/3	0.5	0.28(7)	B_{11}	0.74(13)	$\frac{1}{2}B_{11}$	0.43(6)
Pt2	1a	0	0	0	0.46(9)	B_{11}	-20(20)	$\frac{1}{2}B_{11}$	0.25(8)
Interatomic distances (pm)									
Central atom		Yb		Pt1		Pt2		In	
Ligand atoms		4Pt1	296.6	3In	281.1	6In	273.6	2Pt2	273.6
		3Pt2	304.5	6Yb	296.6	3Yb	304.5	2Pt1	281.1
		2In	313.2					2Yb	313.2
		4In	327.2					4Yb	327.2
		2Yb	376.3					2In	344.1
		4Yb	397.0					2In	376.3

analysis yielded the composition Yb, 31.2 at.%; Pt, 34.9 at.%; In, 33.9 at.%, which was in good agreement with the ideal 1:1:1 stoichiometry. No traces of any impurity elements were observed.

The suitability of the obtained single crystals for x-ray intensity data collection was proved by Laue and rotation techniques using a RKV-86 camera with Mo $K\alpha$ radiation. These studies unambiguously confirmed a hexagonal Laue symmetry of the crystals. X-ray diffraction intensities were recorded employing a four-circle diffractometer DARTCH-1 with a graphite-monochromated Mo $K\alpha$ radiation.

Magnetic measurements were performed on polycrystalline samples in the temperature range 1.7–300 K and in applied magnetic fields up to 5 T employing a Quantum Design MPMS-5 superconducting quantum interference device (SQUID) magnetometer.

The heat capacity was measured in the range 0.2–10 K using a thermal relaxation method.

The temperature and magnetic field dependence of the electrical resistivity was studied in the temperature interval 0.1–300 K and in magnetic fields up to 14 T employing a standard dc four-point technique. The measurements below 4 K were done in a Cryogenics ³He-⁴He dilution refrigerator. The specimens were glued to sapphire supports, and the electrical leads were thin copper wires contacted to the sample by tin soldering.

III. EXPERIMENTAL RESULTS AND DISCUSSION

A. Crystal structure

Refinement of the crystal structure of YbPtIn was performed using a Rietveld-type CSD-program.¹² The starting atomic parameters of the ytterbium and platinum atoms were determined by direct methods, while the indium atoms were located employing a subsequent difference Fourier synthesis. The final difference Fourier map yielded no significant re-

sidual peaks. The final discrepancy factor R was 0.0517 for 138 $|F|$ values and 14 variables. The main crystallographic data are collected in Table I, and the crystal structure is displayed in Fig. 1.

YbPtIn crystallizes with the hexagonal structure of ZrNiAl type (space group $P\bar{6}2m$), which can be considered as an ordered version of Fe₂P type.¹³ The same structure type has previously been reported for the rare earth RPtIn phases with $R = Y, La, Ce, Nd, Gd, Dy, Er, Tm, \text{ and } Lu$.¹⁴ As emphasized in Fig. 1, the ZrNiAl-type structure has a typical layered character with two kinds of atomic sheets which alternate along the c axis. In YbPtIn one of these layers contains Yb and Pt atoms, and the other one In and Pt atoms. Another characteristic structural feature is that the Yb atoms form in YbPtIn a triangular sublattice.

B. Physical properties

The temperature variation of the molar magnetic susceptibility of YbPtIn is presented in Fig. 2. Above 50 K the susceptibility follows a Curie-Weiss law (see the inset to Fig. 2) with the effective magnetic moment $\mu_{\text{eff}}=4.21\mu_B$ and the paramagnetic Curie temperature $\theta_{\text{CW}}=-16$ K. The value of μ_{eff} is somewhat lower than that expected for a free Yb³⁺ ion ($4.54\mu_B$). The negative value of θ_{CW} may suggest anti-ferromagnetic interactions and/or a Kondo effect. Below 50

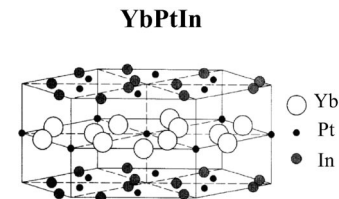


FIG. 1. Crystal structure of YbPtIn (ZrNiAl type).

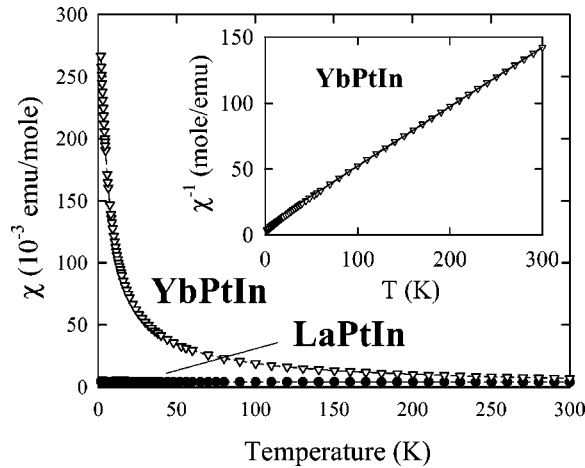


FIG. 2. Temperature dependence of the molar magnetic susceptibility of YbPtIn and LaPtIn. Inset: the inverse susceptibility vs temperature for YbPtIn. The solid line is a Curie-Weiss fit (see text).

K the susceptibility deviates from a straight-line behavior, presumably due to thermal depopulation of the crystal field levels.

As displayed in Fig. 3, the low-temperature magnetic susceptibility of YbPtIn does not show any anomaly down to 1.7 K regardless of whether it is measured in weak or strong magnetic fields. Yet it is worthwhile noting that below about 3.5 K, the susceptibility becomes slightly field dependent. This feature may reflect the onset of some magnetic correlations. At the lowest temperatures studied the magnetization of YbPtIn is initially an almost linear function of the magnetic field but in stronger fields it shows some tendency towards saturation (see Fig. 4). At 1.7 K and in a field of 5 T the magnetic moment is $1.6\mu_B$; i.e., it is much smaller than the free Yb^{3+} ion value of $4\mu_B$. Only above 10 K is the magnetization almost perfectly proportional to the magnetic field. No hysteresis effect in $\sigma(B)$ was observed at any temperature studied.

The featureless low-temperature behavior of $\chi(T)$ and $\sigma(B)$ might suggest that YbPtIn remains paramagnetic at least down to 1.7 K. However, such a presumption is clearly

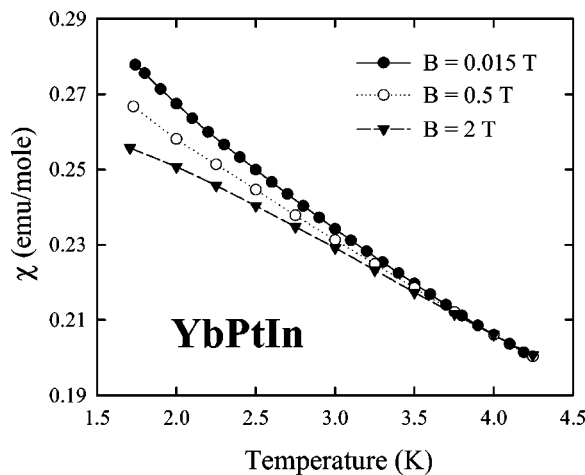


FIG. 3. Low-temperature magnetic susceptibility of YbPtIn measured in various magnetic fields.

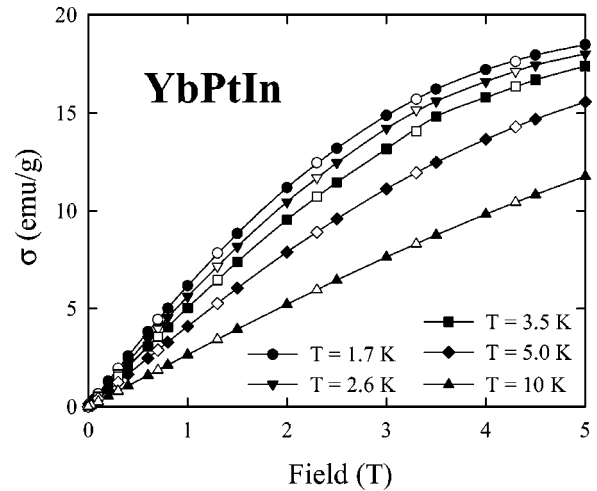


FIG. 4. Field variation of the magnetization of YbPtIn measured at various temperatures with increasing (solid symbols) and decreasing (open symbols) magnetic fields.

contradicted by the heat capacity data, shown in Fig. 5. There, as many as three pronounced anomalies are seen in the low-temperature variation of the specific heat, namely, at 3.1, 2.3, and 1.2 K. The first transition can be associated with the onset of magnetic order. In turn, the other two features have unknown origin. The anomaly at 2.3 K coincides with an antiferromagnetic transition in Yb_2O_3 ,¹⁵ and therefore it may reflect the presence of some small amount (below the detection limit of x-ray powder diffraction) of this parasitic phase. Alternatively, both the 2.3 and 1.2 K anomalies may manifest some order-order type phase transitions; i.e., they may reflect intrinsic magnetic behavior of the compound studied. It is worth recalling at this point that subsequent spin reorientations have also been evidenced in other ternaries crystallizing in the hexagonal ZrNiAl-type structure, e.g., YbPtSn and YbRhSn,¹ and considered as being due to magnetic frustration, which develops between the magnetic ions arranged in a triangular symmetry manner (for a discussion see Refs. 1 and 11).

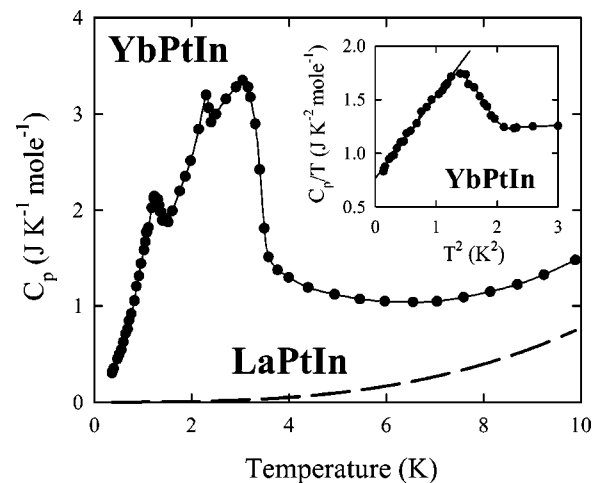


FIG. 5. Temperature dependence of the specific heat of YbPtIn and LaPtIn (the data for LaPtIn taken from Ref. 16). Inset: low-temperature specific heat of YbPtIn in the form C/T vs T^2 . The solid line marks a fit to the function $C/T = \gamma + \beta T^2$ (see text).

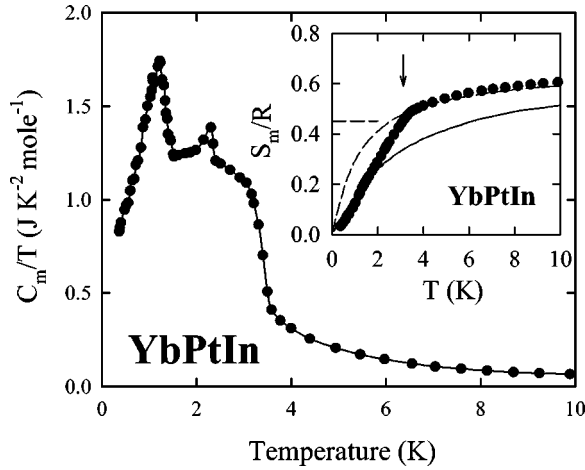


FIG. 6. Temperature dependence of the magnetic specific heat of YbPtIn. Inset: temperature dependence of the magnetic entropy for YbPtIn. The arrow denotes T_N . The solid and dashed lines are theoretical predictions for the single-ion entropy with $T_K=7.7$ and 3.2 K, respectively (see text). The horizontal dashed bar marks the Bethe ansatz solution for S_m at T_K .

As displayed in the inset to Fig. 5 the specific heat data obtained below 1 K can be well approximated by the formula $C/T = \gamma + \beta T^2$, appropriate for antiferromagnetic spin waves. From this equation a strongly enhanced coefficient γ of 740 mJ/mol K² is derived. This value can be compared with $\gamma=500$ mJ/mol K² reported for the isostructural cerium-based counterpart CePtIn.¹⁶ The latter compound, which is a well-established heavy-fermion system, does not, however, order magnetically down to at least 60 mK. In the paramagnetic region the C/T ratio for YbPtIn shows a minimum of about 150 mJ/mol K² around 7 K and this value can be compared with 200 mJ/mol K² measured at the same temperature for CePtIn.¹⁶

In order to derive the magnetic contribution to the total measured specific heat one usually approximates the lattice contribution to $C(T)$ by the specific heat of a nonmagnetic counterpart to the compound studied. In the case of YbPtIn the most appropriate phase would be LuPtIn. However, all our attempts to synthesize this latter compound have failed. Therefore, in the following, another nonmagnetic compound LaPtIn, which crystallizes with the same crystal structure as YbPtIn, is considered as its phonon counterpart. As shown in Fig. 2, LaPtIn is a temperature-independent weak paramagnet with the susceptibility of the order of 10^{-3} emu/mol. The temperature variation of the specific heat of LaPtIn is displayed in Fig. 5. Below 10 K it can be represented by the formula $C/T = \gamma + \beta T^2$ with the Sommerfeld coefficient $\gamma = 0.2$ mJ/mol K² and $\beta = 0.77$ mJ/mol K⁴.¹⁶ The Debye temperature for LaPtIn, derived from the specific heat data, amounts to 196 K. The magnetic heat capacity of YbPtIn, obtained by subtraction from the specific heat of YbPtIn that one of LaPtIn (the latter corrected for the difference in the molar mass of the ytterbium- and lanthanum-based compounds), is shown in Fig. 6 in the form $C_m/T(T)$. The magnetic entropy calculated from this variation (with the assumption of a linear temperature dependence of the specific heat in the range 0–0.3 K) is presented in the inset to Fig. 6. The entropy released at 10 K (the upper limit of our mea-

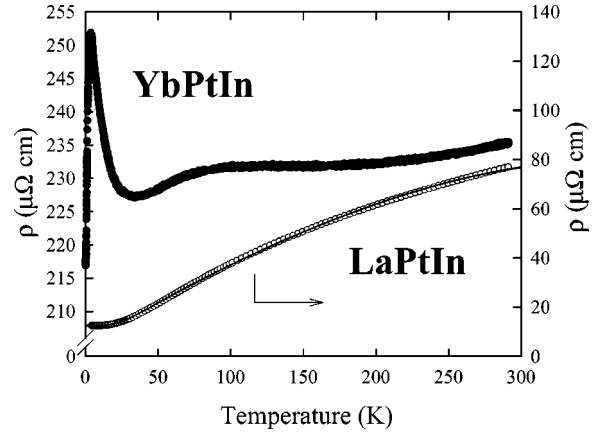


FIG. 7. Temperature variation of the electrical resistivity of YbPtIn and LaPtIn. The solid line is a fit to the Bloch-Grüneisen-Mott expression (see text).

surements) is only $0.88R \ln 2$. In turn, the entropy at T_N is only 66% of the value expected for a doublet ground state. This large reduction of the magnetic entropy may result from a Kondo effect. To examine this hypothesis the experimentally derived $S_m(T)$ was compared with the Bethe ansatz solution obtained for a Kondo impurity ($s=1/2$) by Desgranges and Schotte.¹⁷ In this procedure the Kondo temperature of 7.7 K was taken, as estimated from the low-temperature specific heat data. As is apparent from the inset to Fig. 6, reasonable agreement between the experimental results and theoretical prediction was obtained only at the lowest temperatures ($T < 2$ K). Another comparison can be made assuming $T_K=3.2$ K, as derived from the magnetoresistivity data from the paramagnetic region (see below). In this case a good description of the experimental $S_m(T)$ was obtained above T_N (see the dashed line in the inset to Fig. 6). It is also worthwhile noting that the magnetic entropy released in YbPtIn at 4 K is about $0.65R \ln 2 (=0.45R)$ which, according to the Bethe ansatz solution, should be observed just at T_K .

The temperature variation of the electrical resistivity of YbPtIn is presented in Fig. 7. Above 50 K the resistivity is slightly temperature dependent, showing only a broad local maximum around 90 K. Yet below about 30 K it starts to increase rapidly, goes through a sharp peak at 4 K, and finally drops down rapidly towards lower temperatures. In contrast, the electrical resistivity of LaPtIn exhibits a typical metallic behavior and can be approximated in the whole temperature range by the Bloch-Grüneisen-Mott expression¹⁸

$$\rho(T) = \rho_0 + 4RT \left(\frac{T}{\Theta_D} \right)^4 \int_0^{\Theta_D/T} \frac{x^5 dx}{(e^x - 1)(1 - e^{-x})} - KT^3, \quad (1)$$

with the parameters $\rho_0 = 12 \mu\Omega \text{ cm}$, $R = 0.28 \mu\Omega \text{ cm/K}$, $\Theta_D = 182$ K, and $K = 7.3 \times 10^{-7} \mu\Omega \text{ cm/K}^3$. It is worth noting that the Debye temperature derived for LaPtIn from the resistivity data agrees well with that estimated from the specific heat results (see above). Assuming that the temperature-dependent part of the resistivity of LaPtIn gives a reasonable approximation of the phonon contribution to the total measured resistivity of YbPtIn, the magnetic resistivity of

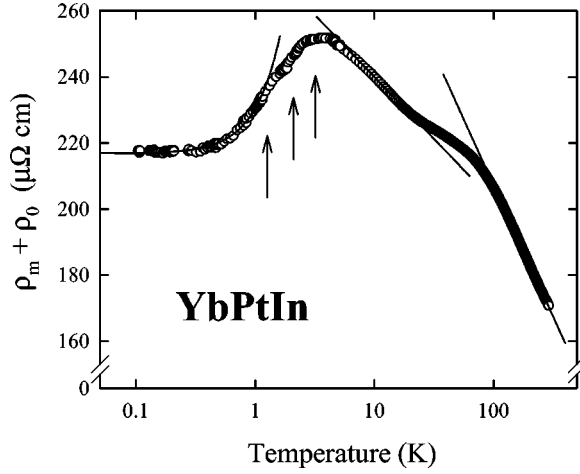


FIG. 8. Temperature variation of the magnetic contribution to the electrical resistivity of YbPtIn. The arrows mark the phase transitions. The solid lines are fits discussed in the text.

YbPtIn was derived (see Fig. 8). In the low-temperature region, over a decade below 1.2 K, the resistivity follows the function

$$\rho_m(T) = \rho_0 + AT^2, \quad (2)$$

with the parameters $\rho_0 = 217 \mu\Omega \text{ cm}$ and $A = 14 \mu\Omega \text{ cm/K}^2$. The transitions at 3.1, 2.3, and 1.2 K are rather hardly seen in $\rho(T)$ but do manifest themselves as singularities in the temperature derivative of the resistivity (not shown). Above 4 K, where the maximum in $\rho(T)$ occurs, the magnetic resistivity exhibits a negative temperature coefficient and shows two distinct regions of logarithmic dependence: between 5 and 30 K, and above 100 K. The fits of the experimental data to the equation

$$\rho_m(T) = a - c_K \ln T \quad (3)$$

yield the following values of the parameters: $a = 278 \mu\Omega \text{ cm}$ and $c_K = 16 \mu\Omega \text{ cm}$ in the range 5–30 K, and $a = 367 \mu\Omega \text{ cm}$ and $c_K = 35 \mu\Omega \text{ cm}$ in the range 100–300 K. The temperature variation of the resistivity of YbPtIn with two logarithmic slopes in the paramagnetic region recalls that characteristic of archetypal Kondo lattices, which exhibit an interplay of Kondo and crystal field interactions.¹⁹ Accordingly, the crystal field splitting in YbPtIn can be estimated from $\rho_m(T)$ as being of about 90 K.

The low-temperature transverse magnetoresistivity ($B \perp i$) of YbPtIn, defined as

$$\frac{\Delta\rho}{\rho}(B, T) = \frac{\rho(B, T) - \rho(B=0, T)}{\rho(B=0, T)}, \quad (4)$$

was measured as a function of magnetic field (see Fig. 9) and temperature (see Fig. 10) down to 100 mK and in magnetic fields up to 14 T. The magnetoresistivity is negative except in fields lower than 1.5 T. A characteristic anomaly in the magnetoresistivity occurring in fields around 4 T might be related to a kind of metamagnetic-type transformation, though no corresponding feature was observed in the field-dependent magnetization (compare Fig. 4). The largest magnetoresistivity of about -35% is observed at the Néel temperature in a field of 14 T, where a minimum in $\Delta\rho/\rho(T)$

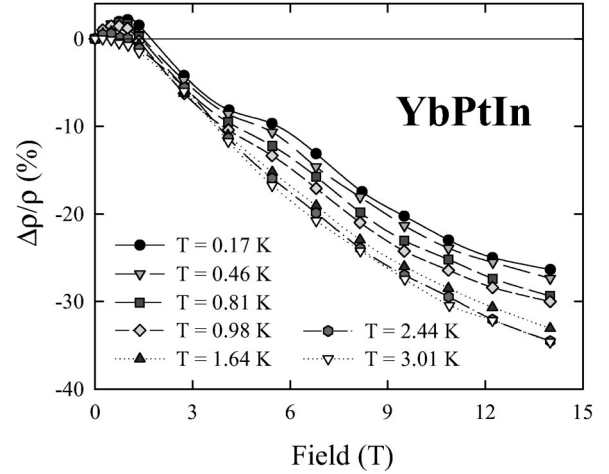


FIG. 9. Field dependence of the transverse magnetoresistance of YbPtIn measured at various temperatures below T_N .

occurs. Yet also well above T_N the magnetoresistivity of YbPtIn is quite large. For example, the negative magnetoresistance taken in $B = 8 \text{ T}$ becomes smaller than 1% only above about 60 K. Figure 11 displays the electrical resistivity of YbPtIn measured as a function of temperature in the paramagnetic region at various applied magnetic fields. With increasing field the low-temperature maximum in the resistivity (occurring at 4 K in zero field) gradually broadens and shifts to higher temperatures. At 8 T the maximum is already hardly seen. In Fig. 12 the magnetoresistivity of YbPtIn measured as a function of magnetic field in the paramagnetic region is shown. The overall character of these $\Delta\rho/\rho(B)$ curves is reminiscent of that characteristic of Kondo impurities. Thus, in order to test a single-ion scaling relation, applied previously to several well-established heavy-fermion systems,²⁰ the magnetoresistivity data were replotted as a function of $B/(T + T^*)$. The result obtained assuming a characteristic temperature T^* of 4 K is presented in Fig. 13. Apparently, all the magnetoresistance curves measured at different temperatures are superimposed there on a single curve. It is worth noting that reducing or increasing T^* by 0.5 K makes this overlap considerably worse. Such a good

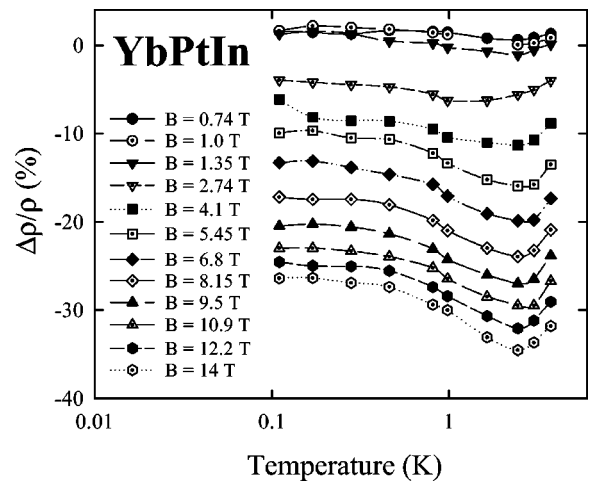


FIG. 10. Low-temperature dependence of the transverse magnetoresistance of YbPtIn taken in various magnetic fields.

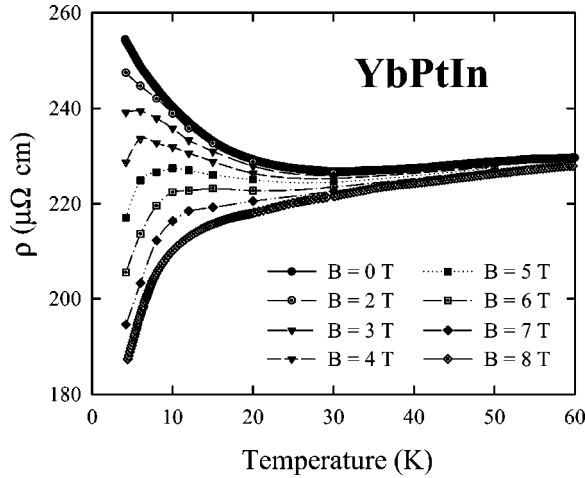


FIG. 11. Temperature dependence of the electrical resistivity of YbPtIn measured above T_N in various magnetic fields.

applicability of the Kondo scaling to YbPtIn strongly supports classifying this compound as a dense Kondo system.

Another indication of Kondo behavior in YbPtIn comes from analysis of the magnetoresistivity data in terms of Friedel's sum rule. According to Schlottmann,²¹ who applied the Bethe ansatz technique in order to calculate within the Coqblin-Schrieffer model the zero-temperature magnetoresistivity of a Kondo impurity, the ratio $\rho(B)/\rho(B=0)$ can be expressed as

$$\frac{\rho(B=0)}{\rho(B)} = \frac{1}{2j+1} \sum_{i=1}^{2j+1} \sin^{-2}\left(\frac{\pi n_i}{2j+1}\right), \quad (5)$$

where the occupation number n_i of the $2j+1$ Zeeman levels generated by the magnetic field is constrained by

$$\sum_{i=1}^{2j+1} n_i = 1. \quad (6)$$

The model predicts a negative magnetoresistivity $\Delta\rho/\rho(B)$, which depends universally on a single energy scale B^* , re-

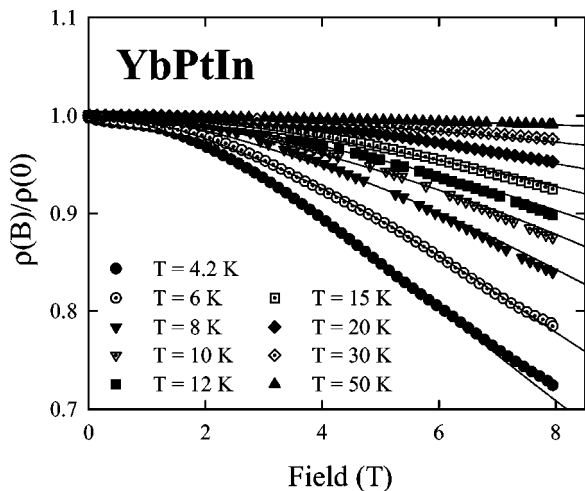


FIG. 12. Field variation of the transverse magnetoresistance of YbPtIn, presented as $\rho(B)/\rho(B=0)$, measured at various temperatures above T_N . The solid lines are fits to the Schlottmann expression (see text).

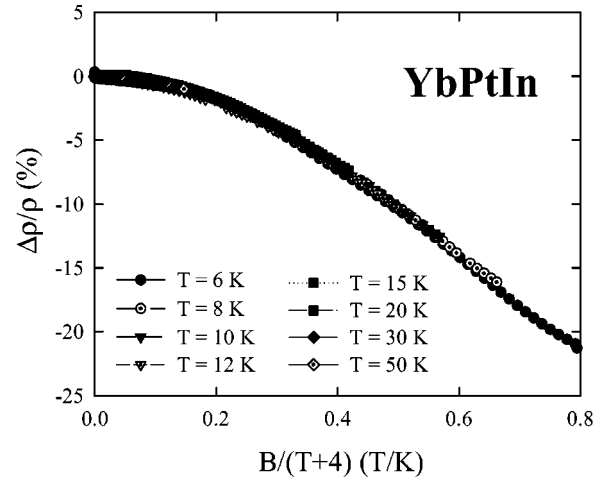


FIG. 13. Single-ion scaling (see text) of the transverse magnetoresistance of YbPtIn.

lated to the Kondo temperature. In order to apply Schlottmann's theory to YbPtIn measured at finite temperatures, the parameter B^* was adjusted in such a way as to get the best fit of the universal curve (taken from Ref. 21) to the experimental data. The results of the fitting are shown in Fig. 12 by the solid lines. The values of the characteristic field B^* derived from these fits are plotted in Fig. 14 as a function of temperature. According to Battlog *et al.*,²² $B^*(T)$ is a linear function of temperature and follows the formula

$$B^*(T) = B^*(0) + \frac{k_B}{g\mu} T = B^*(0) \left(1 + \frac{T}{T_K}\right), \quad (7)$$

where μ is the Kondo-screened magnetic moment and g stands for the Lande factor. Applying this relation to the data of YbPtIn one gets $\mu = 0.4\mu_B$ (for $g = 8/7$ appropriate for Yb^{3+} ion) and $T_K = 3.2$ K, the latter value being in reasonable agreement with the other estimates.

IV. SUMMARY

The hexagonal compound CePtIn is a well-known paramagnetic heavy-fermion system.¹⁶ We attempted to investi-

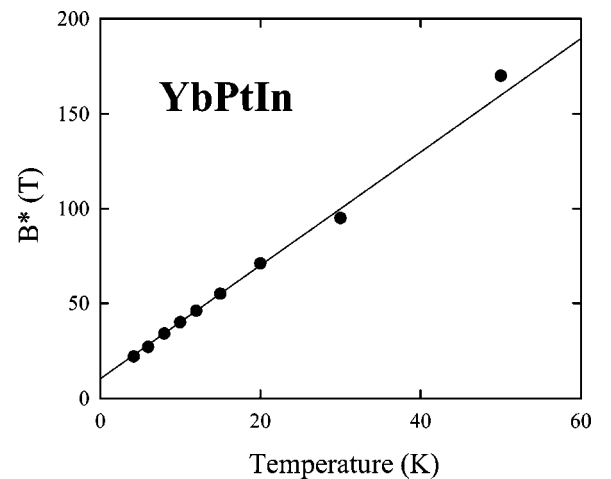


FIG. 14. Temperature variation of the characteristic parameter B^* (see text) as derived from the fits presented in Fig. 12.

gate an ytterbium-based counterpart and prepared YbPtIn. The x-ray diffraction study, performed on a single crystal, has revealed that the new compound is indeed isostructural to CePtIn, adopting a crystallographic unit cell of ZrNiAl type. The magnetic measurements have indicated in YbPtIn the presence of almost trivalent Yb ions which carry rather well-localized magnetic moments. The heat capacity measurements have shown that the ytterbium indide orders magnetically at 3.1 K. Two further λ -type anomalies in $C(T)$ have been observed at lower temperatures, the origin of which is unclear as yet. The magnetic entropy in YbPtIn is strongly reduced with respect to the value characteristic of a doublet ground state. Moreover, the C/T ratio extrapolated to 0 K attains as large a value as about 700 mJ/mol K². The electrical resistivity of YbPtIn exhibits a T^2 behavior at low temperatures and a $\ln T$ dependence in the paramagnetic re-

gion. The transverse magnetoresistivity is negative and rather large.

All the experimental findings strongly suggest that YbPtIn is a magnetically ordered dense Kondo system with pronounced crystal field effects. This presumption is supported by the results of semiquantitative analysis of our experimental data in terms of Kondo scaling. The theoretical predictions describe remarkably well the measured heat capacity, resistivity, and magnetoresistivity of YbPtIn, yielding a characteristic temperature of about 4 K.

ACKNOWLEDGMENT

The work at the University of Florida was supported by the Department of Energy under Contract No. DE-FG02-99ER45748.

*Author to whom correspondence should be addressed.

- ¹D. Kaczorowski, A. Leithe-Jasper, P. Rogl, H. Flandorfer, T. Cichorek, R. Pietri, and B. Andraka, *Phys. Rev. B* **60**, 422 (1999).
- ²J. C. P. Klaasse, W. C. M. Mattens, F. R. de Boer, and P. F. de Châtel, *Physica B* **86-88**, 234 (1977).
- ³S. Cirafizi, A. Palenzona, and F. Canepa, *J. Less-Common Met.* **107**, 179 (1985).
- ⁴P. Bonville, P. Bellot, J. A. Hodges, P. Imbert, G. Jehanno, G. Le Bras, J. Hammann, L. Leylekian, G. Chevrier, P. Thuery, L. D'Onofrio, A. Hamzic, and A. Barthelemy, *Physica B* **182**, 105 (1992).
- ⁵D. T. Adroja, B. D. Rainford, S. K. Malik, M. Gailloux, and K. A. Gschneidner, Jr., *Phys. Rev. B* **50**, 248 (1994).
- ⁶C. Schank, G. Olesch, J. Köhler, U. Tegel, U. Klinger, J. Diehl, S. Klimm, G. Sparn, S. Horn, C. Geibel, and F. Steglich, *J. Magn. Mater.* **140-144**, 1237 (1995); J. Diehl, H. Davideit, S. Klimm, U. Tegel, C. Geibel, F. Steglich, and S. Horn, *Physica B* **206&207**, 344 (1995).
- ⁷S. K. Dhar, N. Nambudripad, and R. Vijayaraghavan, *J. Phys. F: Met. Phys.* **18**, L41 (1988); P. Bonville, G. Le Bras, P. Dalmas de Reotier, A. Yaouanc, R. Calemczuk, C. Paulsen, M. Kasaya, and F. G. Aliev, *Physica B* **230-232**, 266 (1997).
- ⁸G. Le Bras, P. Bonville, J. A. Hodges, J. Hammann, M. J. Besnus, G. Schmerber, S. K. Dhar, F. G. Aliev, and G. Andre, *J. Phys.: Condens. Matter* **7**, 5665 (1995).
- ⁹M. F. Hundley, J. D. Thompson, P. C. Canfield, and Z. Fisk, *Phys. Rev. B* **56**, 8098 (1997), and references cited therein.
- ¹⁰D. Kaczorowski, B. Andraka, V. I. Zaremba, and Cz. Marucha, *Physica B* **281&282**, 44 (2000).
- ¹¹O. Trovarelli *et al.* (unpublished).
- ¹²L. G. Akselrud, Yu. N. Grin, P. Yu. Zavalij, V. K. Pecharsky, and V. S. Fundamentalsky (unpublished).
- ¹³P. I. Kryp'yakevich, V. Ya. Markiv, and Ya. V. Melnyk, *Dopov. Akad. Nauk. Ukr. RSR, Ser. A: Fiz.-Tekh. Mat. Nauki* **8**, 750 (1967).
- ¹⁴R. Ferro, R. Marazza, and G. Rambaldi, *Z. Anorg. Allg. Chem.* **410**, 219 (1974); D. Rossi, D. Massone, R. Marazza, and R. Ferro, *ibid.* **507**, 235 (1983).
- ¹⁵J. C. P. Klaasse, J. W. E. Stekenburg, A. M. H. Bleyendaal, and F. R. de Boer, *Solid State Commun.* **13**, 561 (1973).
- ¹⁶K. Satoh, T. Fujita, Y. Maeno, Y. Uwatoko, and H. Fujii, *J. Phys. Soc. Jpn.* **59**, 692 (1990).
- ¹⁷H. U. Desgranges and K. D. Schotte, *Phys. Lett.* **91A**, 240 (1982).
- ¹⁸N. F. Mott and H. Jones, *The Theory of the Properties of Metals and Alloys* (Oxford University Press, New York, 1958), p. 240.
- ¹⁹D. Cornut and B. Coqblin, *Phys. Rev. B* **5**, 4541 (1972).
- ²⁰B. Andraka and G. R. Stewart, *Phys. Rev. B* **49**, 12 359 (1994); B. Andraka, *ibid.* **52**, 16 031 (1995).
- ²¹P. Schlottmann, *Z. Phys. B: Condens. Matter* **51**, 223 (1983); *Phys. Rev. B* **35**, 5279 (1987).
- ²²B. Batlogg, D. J. Bishop, E. Bucher, B. Golding, A. P. Ramirez, Z. Fisk, J. L. Smith, and H. R. Ott, *J. Magn. Mater.* **63&64**, 441 (1987).